Online Resource 1

Supplementary material for *A Spatial Model of Chronic Wasting Disease and the Optimal Placement of a Sight-Based Cull*

Bulletin of Mathematical Biology

Gabe Flanagin* Alex Escoto
Zhen Chao

Department of Mathematics, Western Washington University, Bellingham, WA, USA

Numbers prefixed S are internal to this document, and every other cross-reference points into the main text. Section S1 gives the readings behind the parameter values of Section 2, and Section S2 explains the design of the sweep. Section S3 describes the landscape meshes and gives the full ablation, and Section S4 gives the verification, the per-cell baselines and the robustness checks.

S1 Parameter Provenance

This section records how each value in Table 1 was reached, including unit conversions and why some sources were set aside.

S1.1 Carrying capacity K_0

Three readings bracket K_0, and none is direct. Geremia et al. (2015) monitor roughly 7,300 deer over 4,600 km^2, a landscape mean of 1.6 deer/km^2 at capacity, while Miller et al. (2006) work with carrying capacities of 0–1 deer/km^2. Since K_0 is the capacity of the best cover class and every other class is scaled down by $c(\mathbf{x}) \leq 1$, a landscape mean near 1.6 implies a best-class value of roughly 2–3. The third reading comes from a census rather than a model. Suresh et al. (2026) divide a statewide agency estimate of 707,000 deer among 646 cells of 400 km^2 to obtain 2.6 deer/km^2 across Kansas, which at the landscape means $\bar{c} = 0.78$–0.84 of our meshes corresponds to $K_0 = 3.1$–3.3. This agreement should not be pressed far, since the Kansas herd is mostly white-tailed deer on a different landscape, and a statewide total divided by area is a standing density rather than a carrying capacity. Still, it is the only one of the three readings drawn from an agency population survey, and it moves $K_0 = 3$ from the upper edge of the bracket into its interior.

S1.2 Intrinsic growth rate r

The logistic term needs the $N \to 0$ limit of the per-capita rate $r(1 - N/K)$, so a growth rate realized on a standing herd would need correcting upward by $1/(1 - N/K)$. The mule deer figures adopted here need no correction, because they are not realized rates. Almberg et al. (2011) report a maximum annual finite growth rate of $\lambda = 1.30$ for their mule deer demography and compare it with the 1.16–1.27 that Tanner (1975) estimated for wild mule deer as dominant eigenvalues of Leslie matrices built from the highest observed survival and fertility schedules. A life-table λ built

*Corresponding author: flanagg@wwu.edu

from best-observed vital rates is already the density-free asymptotic rate. We take the logarithm of Almberg et al.'s figure, the larger of the two, giving $r = \ln 1.30 = 0.26$ yr^{-1}. Geremia et al. (2015) fit $\lambda = 1.01$ (0.95–1.07) in the absence of CWD, but that herd is hunted at its carrying capacity, where $\lambda \approx 1$ by definition, so it constrains K rather than the intrinsic rate.

S1.3 Diffusivity κ

Since front speeds scale as $\sqrt{\kappa}$, an observed speed u_{obs} requires $\kappa = 4\,(u_{\text{obs}}/1.6)^2$ km^2/yr, where 1.6 km/yr is the uncontrolled leading-edge speed at ($\delta = 0.25,\ R_0 = 3.5$) on the sweep disk. Suresh et al. (2026) track weighted centroids of simulated infection through nineteen years of Kansas surveillance and report zonal rates of 1.60 km/yr in the northwest, 2.59 in the southwest and 3.21 in the north-central zone, which require $\kappa \approx 4$, 10 and 16. They attribute the two larger figures, in the south-central and eastern zones, to sparse sampling rather than sustained advance, and they read the northwestern zone as a persistent source region rather than an advancing front. Its displacement is therefore the least likely to be an artifact of detection order, and it is the rate we calibrate to. The match holds only to order of magnitude, since the weighted-centroid displacement of an established cluster on a 20 km grid is not a traveling-wave speed. Garlick et al. (2014) obtain 3.7–5.5 km/yr for mule deer in southeastern Utah, which would need $\kappa \approx 21$–47. Their faster figures, up to 11 km/yr, are computed at the management objective population rather than the estimated one and are not the right comparison.

The gap against Garlick et al. admits two readings, and we do not decide between them. The first is structural. Fickian diffusion with a single coefficient cannot reproduce spread driven by a fat-tailed kernel, so frontal advance here is a lower bound. The second is that κ is simply too small, and their movement data support this. Their homogenized diffusion coefficient is the harmonic mean of motility (their Eq. 47), and the area-weighted harmonic mean of their winter motilities over the dominant cover classes is roughly 70–90 km^2/yr, an order of magnitude above our value and of the same order as the 21–47 their spread rates require. Those motilities come from GPS telemetry on the right species, which is stronger evidence than anything behind our value. They are also measured on Colorado Plateau shrubland under a different land-cover classification, however, so they do not transfer to a subalpine mesh without a crosswalk of unknown loss. Resolving this means enlarging the domain with the diffusivity, for the reason given in Section S2.

Step-level telemetry cannot close the gap either. The four-hour step lengths of the 596 collared white-tailed deer of Gilbertson et al. (2025) in southwestern Wisconsin give a step-level $\mathbb{E}[L^2]/4\Delta t$ of 52–178 km^2/yr, but this measures foraging within a home range, whereas the diffusion tensor needs the population's effective dispersal, set by the drift of home-range centroids. Collar data analyzed for that drift are what should eventually replace κ.

S1.4 Land-cover coefficients

Table S1 gives the coefficients for every class, and Section 2.5 explains why c and p come from different sources.

For permeability, Mandujano Reyes et al. (2025) fit a divergence-form Fisher–KPP model to 76,717 CWD test results from white-tailed deer in Wisconsin, with NLCD class indicators in the log-diffusion coefficient, so their class-to-class ratios transfer directly. We set $p \propto \exp(\alpha_{\text{class}})$ over the terrestrial classes, normalized to the largest. Forest, shrub and grassland lie at 0.62–1.0 while pasture and hay sit at 0.15, which is the informative gap, although it is the least constrained of the significant coefficients, with a 95% interval that maps to $p \in [0.02, 0.55]$. Their coefficient describes the spread of prevalence rather than deer movement, so part of this gap may reflect the

low deer density that c already carries. We do not take two classes from the fit. Open water implies $p \approx 0.20$, which is plausible for streams at 30 m resolution but wrong for the water bodies on our meshes, so we set $p = 0.01$, nonzero only to keep (9) nonsingular. The developed-land coefficient is about fourteen times the terrestrial maximum, most likely because human-mediated spread has been absorbed into a movement coefficient, so we instead impose a gradient that decreases with development intensity, [ASM] but with the sign empirically supported.

For habitat quality, the growth-rate coefficients of Mandujano Reyes et al. are not suitable, since they measure transmission intensity rather than density and fail empirically as a habitat index. Their rank correlation with habitat quality is +0.17, and the largest belongs to emergent herbaceous wetlands, a class that supports few deer. We instead use the ecological-diffusion model of Garlick et al. (2014), whose per-cover motilities come from mule deer GPS collars and whose steady state $\hat{S} = C/\mu$ makes relative density proportional to $1/\mu$. We combine male and female winter values at the reported 15 bucks per 100 does, and aggregate LANDFIRE types to NLCD classes by the area-weighted mean of $1/\mu$. Only the five classes covering 91% of their study area have enough GPS data to adopt. Since residence time measures use rather than capacity, we also override their values for barren land (0.49) and open water (0.97), which reflect escape terrain and misclassified dry washes. Codes absent from the table default to 0.5 in both columns.

Table S1: Land cover coefficients, keyed to NLCD/MRLC class codes, grouped by provenance rather than by code. Column c is the carrying-capacity scaling of Section 2.4, column p the permeability multiplier in (9) normalized to 1.0 at the most permeable class. [LIT] entries of c come from the mule deer motilities of Garlick et al. (2014) and of p from the log-diffusion coefficients of Mandujano Reyes et al. (2025), † marking a coefficient whose 95% interval contains zero and ‡ one whose interval spans more than an order of magnitude in p. Shaded rows carry at least one assumed value.

Code	Land cover class	c (habitat)	p (permeability)	c src	p src
0	Unknown or nodata	0.50	0.50	[ASM]	[ASM]
11	Open water	0.00	0.01	[ASM]	[ASM]
12	Perennial ice or snow	0.00	0.30	[ASM]	[ASM]
21	Developed, open space	0.50	0.90	[ASM]	[ASM]
22	Developed, low intensity	0.35	0.70	[ASM]	[ASM]
23	Developed, medium intensity	0.15	0.40	[ASM]	[ASM]
24	Developed, high intensity	0.03	0.10	[ASM]	[ASM]
31	Barren land	0.10	0.90	[ASM]	[ASM]
43	Mixed forest	0.80	0.76	[ASM]	[LIT]†
81	Pasture or hay	0.60	0.15	[ASM]	[LIT]‡
82	Cultivated crops	0.35	0.57	[ASM]	[LIT]†
95	Emergent herbaceous wetlands	0.30	0.46	[ASM]	[LIT]
41	Deciduous forest	0.75	1.00	[LIT]	[LIT]†
42	Evergreen forest	0.85	0.62	[LIT]	[LIT]
52	Shrub or scrub	1.00	0.81	[LIT]	[LIT]
71	Grassland or herbaceous	0.80	0.80	[LIT]	[LIT]
90	Woody wetlands	0.95	0.73	[LIT]	[LIT]

S1.5 Stage durations

Miller et al. (2006), as reported by Sharp and Pastor (2011), give 1.76 yr from infection to death. Geremia et al. (2015) give about 1.5 yr from post-infection annual survivals of 0.68, 0.41 and 0.18,

Potapov et al. (2016) about 2 yr, and Miller et al. (2008) 1.6 yr of additional life expectancy in the Table Mesa cohort. The adopted 1.75 yr sits near the center of this 1.5–2.1 yr spread.

S1.6 Environmental persistence δ

The published decay rates of Section 2.8 reach us in different forms. The system of Miller et al. (2006) arrives through two renderings that disagree by an order of magnitude, and neither figure is that paper's own estimate. Sharp and Pastor (2011) adopt soil residence times of three and ten years to illustrate their critical carrying capacity, giving $\delta \in [0.10, 0.33]$ yr^{-1}, while Garlick et al. (2014) tabulate $\delta = 0.007$ day$^{-1} = 2.56$ yr^{-1} and attribute it to Miller et al. directly. The reference value $\delta = 0.15$ at which the route split of Section 2.9 is set lies at the persistent end, so a reader who prefers Garlick et al.'s reading should treat that split as an upper bound on the environmental share. Almberg et al. (2011) sweep weekly prion survival probabilities s from 0.9481 to 0.9983, which they report as half-lives of 0.25 to 8 yr and which convert to $\delta = -52 \ln s \in [0.089, 2.77]$ yr^{-1}. Potapov et al. (2016) argue that prions become practically inaccessible after one to two years, which we read as $\delta \approx 0.5$–1.0 yr^{-1}.

S1.7 Field readings of R_0

Geremia et al. (2015) report female CWD prevalence of 0.08 (0.06–0.11) in 1997–2002 and 0.04 (0.02–0.07) in 2010–11, together with an annual infection probability of 0.04 (0.02–0.07). Inverting (15) against each gives $R_0 = 1.34$, 1.15 and 1.27. The incidence reading falls between the two prevalence readings, which is a real cross-check since the three are reported separately. The inversion does not depend on K_0, since $S^* = K_0/\widetilde{R_0}$ scales out of it, so the least certain parameter does not contaminate it. It is sensitive to r, and not in the intuitive direction, since a slower intrinsic rate sustains a given prevalence only at a larger R_0. The inversion does not settle the question in any case, because over three decades from a localized focus the model follows the transient invasion and never approaches the endemic state the inversion describes.

S1.8 A structural ceiling on prevalence

Prevalence here is limited by recruitment rather than by transmission. By (15), $S^* = K_0/\widetilde{R_0}$, while the infected classes together hold the infection rate F for the mean time from infection to death, $\bar{t} = 1/\sigma_1 + 1/\sigma_2 + 1/\alpha = 1.75$ yr. As $\widetilde{R_0} \to \infty$, $F \sim rK_0/\widetilde{R_0}$, so endemic prevalence saturates at $r\bar{t}/(1 + r\bar{t}) = 31\%$. The 43% that DeVivo et al. (2017) recorded in male mule deer in Wyoming, against 24% overall, is thus out of reach for an unstructured model of this form at any transmission rate. We attribute the gap to the absence of age and sex structure. Field prevalences are measured on harvested adults while N counts every animal, and in a structured herd prevalence concentrates in the older animals that surveillance samples.

S2 Design of the Sweep

This section explains why the grid of Section 7.1 varies the two quantities it does, and how the control weights and the effort cap were fixed.

S2.1 The δ axis

The δ axis is the treatment variable of a designed experiment rather than a sensitivity check on an uncertain parameter, so it needs an argument that the remaining parameters do not confound it. The rescaling of β_2 by (14) supplies one. The alternative, varying δ at fixed β_2, moves the epidemic threshold as a side effect. With β_2 frozen at its $\delta = 0.25$ value, the system at the low anchor $R_0 = 2$ is subcritical by $\delta = 0.60$, so the epizootic would die partway along the range and the upper rungs of the ladder would measure extinction rather than a shorter generation interval. Rescaling instead holds R_0, the route split and the host endemic equilibrium identical at every point, so the sweep isolates the reservoir's memory. In a persistent reservoir each prion unit is weakly infectious but lingers $1/\delta$ years, while in a fast-decaying one each unit is potent but short-lived.

S2.2 The R_0 axis

Both components of (12) are linear in $K = K_0 c(\mathbf{x})$, so sweeping R_0 at fixed K_0 and sweeping K_0 at fixed transmission coefficients expose the herd to the same transmission. This is why K_0, although [ASM], gets no axis of its own. The equivalence is incomplete, since K_0 also sets the logistic ceiling and with it S_∞ and the deficit running cost, but it covers the larger part.

S2.3 The diffusivity

The diffusivity is held fixed, but on the disk this loses nothing, since there κ only sets the length scale. With $c = p = 1$, every host tensor is a constant multiple of κ times the identity, so writing $\mathbf{x} = \lambda\boldsymbol{\xi}$ with $\lambda = \sqrt{\kappa'/\kappa}$ turns the model at κ' on a disk of radius L into the model at κ on a disk of radius L/λ, with the seed width ς of (53) divided by λ. Densities are unchanged pointwise and every area integral is divided by λ^2. The objective is divided as a whole, which leaves its minimizer unchanged, while the detection threshold (54), also an area integral, becomes $R_{\mathrm{det}}/\lambda^2$. Every time and percentage in Tables S6 and 4 therefore holds at any κ', every distance and speed scales by λ, including the offset of the effort ring, and every count of animals scales by λ^2. Our disk at $\kappa = 4$ is also the disk at $\kappa' = 47$, the upper end of the spread rates of Garlick et al. (2014), with $L = 137$ km, $\varsigma = 1.7$ km and $R_{\mathrm{det}} = 714$ clinical deer-years.

The landscapes do not rescale this way, since terrain and land cover do not stretch with κ. There κ sets the diffusion length $\sqrt{\kappa/r} = 3.92$ km against the width of valleys and habitat patches, so the results of Section 7.5 are conditional on it in a way the disk results are not. A κ axis on a landscape also needs a matched domain axis, because raising κ at fixed extent brings the invasion to the boundary within a few years, after which the no-flux condition rather than the landscape determines where the front is. Matching the spread rates of Garlick et al. would need each 100 km box to grow to 230–340 km on a side, five to twelve times the area.

S2.4 The control weights and the effort cap

Since c_3 prices effort and c_4 sets its support, both are held fixed, so the grid measures δ and R_0 rather than the weights, and realized mean effort is reported as an output at every cell.

The capacity $v_{\max} = 3$ is our estimate of what a sustained cull at full effort could achieve, taking $v_{\max}/(v_{\max} + \alpha) = 53\%$ of clinical animals before they die. We also tested $v_{\max} = 2$, which takes 43%. At $c_3 = c_4 = 0.5$ it left up to 41.5% of space–time on the bound, so at the most saturated cells the cap rather than the objective chose the policy. Table S2 gives the saturation at these two cells. At $v_{\max} = 2$, raising c_3 to 1 brings the bound share to about 5%, and at $v_{\max} = 3$, $c_3 = 0.5$ already does, with at most 4.3% on the bound across the sweep (Section S4). We keep $c_3 = 0.5$, since a larger c_3 makes effort dearer at every cell while the cap binds at only a few.

Table S2: The saturation probe: percentage of space–time at $v = v_{\max}$ at the two most saturated cells, at $c_4 = 0.5$.

c_3	$v_{\max}$	$(\delta = 0.125,\ R_0 = 5)$	$(\delta = 1,\ R_0 = 2)$
0.5	2	21.7	41.5
1	2	3.5	5.1
2	2	0.0	0.0

S3 The Landscape Meshes

This section describes the three meshes of Section 7.5 and gives the full results of the ablation.

Each mesh is a 100×100 km square in UTM zone 13N, centered on its focus as far as our elevation and land-cover data allow (Table S3). Terrain is the USGS 3DEP 1/3 arc-second DEM (U.S. Geological Survey, 2024a), mosaicked and resampled bilinearly to a 30 m grid. Land cover is the 2025 layer of Annual NLCD Collection 1, version 1.2 (U.S. Geological Survey, 2024b), sampled by nearest neighbor at the mesh nodes in its native projection, since resampling a categorical raster displaces class boundaries. Node areas span a factor of 4–5 $\times 10^4$ on each mesh, so every control statistic is weighted by lumped mass in space and by block span in time. Evergreen forest, shrub, grassland and deciduous forest cover 82–91% of each mesh (Table 2). The rest is mostly barren ground and wetlands, with developed land and cropland around Estes Park, and no other class exceeds 5% of any mesh. Smoothing $c(\mathbf{x})$ with a Gaussian at the flat-ground diffusion length $\sqrt{\kappa/r} = 3.92$ km, roughly what the diffusion operator does to K, keeps 30% of its variance around Estes Park but only 11% and 9% on the other two meshes.

Table S3: The three landscape meshes. Elevations are at the mesh nodes, after smoothing. Shares, means and percentiles are weighted by surface area, and $\overline{\eta}$ is the area-weighted mean slope factor (10).

	Upper Arkansas	Carbondale	Estes Park
Longitude (°W)	106.77–105.60	107.83–106.64	106.20–105.01
Latitude (°N)	38.26–39.17	39.01–39.93	40.00–40.91
Elevation (m)	1887–4389	1603–4301	1479–4346
Area above 3500 m	14.6%	4.1%	3.8%
Surface (km^2)	10,281	10,324	10,220
Nodes	350,315	370,354	323,798
Triangles	675,541	715,944	622,585
$\overline{\eta}$	0.49	0.43	0.54
$\overline{c}$	0.826	0.837	0.778
$\overline{p}$	0.725	0.777	0.699

The Upper Arkansas mesh is centered on the upper Arkansas valley in Chaffee County, between the Sawatch Range to the west and the Mosquito Range to the east, and reaches into South Park. The focus lies on the valley floor near Nathrop (Figure 4), and evergreen forest and shrub cover 70% of the surface. We use it to illustrate the mechanisms rather than as a study region, since 15% of it lies above 3500 m and so it is not winter range in the sense that Section 8 reads Γ.

The Carbondale mesh covers the Roaring Fork valley and its tributaries, from the Colorado River at Glenwood Springs to the Elk Mountains. The focus sits at the mouth of the Crystal River valley, 2.7 km south-southwest of Carbondale (Figure S1). Evergreen forest, shrub and deciduous forest, all with $c \geq 0.75$, cover nine-tenths of the surface. It is the same kind of landscape as the Upper Arkansas, but steeper and lower, with the lowest $\overline{\eta}$ of the three and less than a third of the high ground.

The Estes Park mesh spans the Front Range across the Continental Divide, from Lake Granby in the west through Rocky Mountain National Park to the edge of the plains in the east. The focus lies 2.1 km north of the town of Estes Park, in shrub, evergreen forest and grassland (Figure 5). Developed land (6.2%) and cultivated crops and pasture (3.8%) lie mostly along the foothills and plains, and these are what give the mesh its land-cover contrast and the lowest $\overline{c}$ of the three. They

are also the classes whose coefficients are least constrained (Section S1.4), so this mesh tests the land cover as much as it demonstrates it.

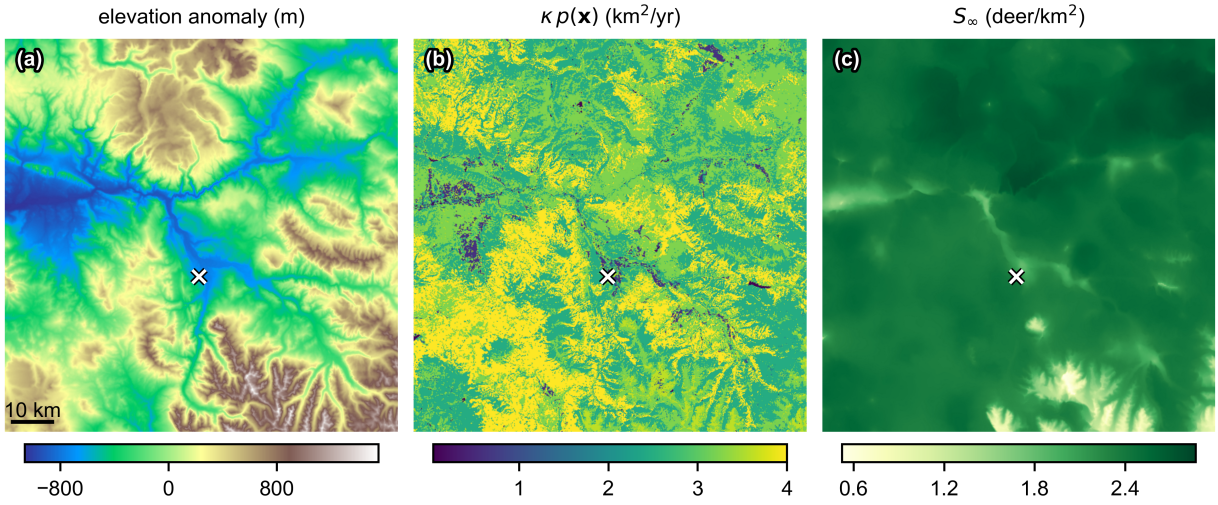


Figure S1: The Carbondale mesh, on the same terms as Figure 4.

Binned by local relief, the ratio of $|\nabla S_\infty|$ between the anisotropic and isotropic arms is 0.96–0.97 below 100 m/km on all three meshes, 1.63–1.73 at 250–400 m/km and 3.84–4.06 above 600 m/km. With the land cover flattened, K is uniform and so is S_∞, so the tensor can sharpen S_∞ only across land-cover boundaries.

Table S4 gives all twelve runs. Each arm reaches the detection threshold (54) at its own time, and the measured land cover delays detection by 0.15–1.85 yr. Across the four arms, deficit reduction spans 0.9 points on the Upper Arkansas, 1.8 on Carbondale and 3.7 around Estes Park. Within each land-cover pair, isotropic diffusion does slightly better than the slope tensor, by 0.8–1.2 points. Only around Estes Park does the land cover cost benefit. There the full model is the worst of its four arms, and flattening the land cover gains 2.4–2.7 points. This is consistent with Estes Park keeping the most land-cover variance, so that its best habitat forms patches large enough for the local $\bar{R}_0 = 4.50$, rather than the average of 3.5, to govern the invasion.

The full model reaches its benefit with 0.36–0.47 yr^{-1} of mean effort against 0.56–0.64 with neither mechanism, and so recovers 1.35–1.44 times as many points of deficit per unit effort. It also leaves the most ground untreated for all twenty years, 53–63% of the mesh against 37–41% with neither mechanism. Much of this ground lies beyond the invasion's reach on a 100 km mesh, so these shares compare arms rather than measure sparsity. The boundary enters only at the end of the control horizon, since uncontrolled fronts first reach an edge about 20–28 yr after handover, and controlled fronts 23–30 yr after.

The anisotropic and isotropic policies share their broad shape, with time-mean controls correlated at 0.95–0.97, but they differ locally by an RMS of 43–71% of the mean, and with the land cover measured the tensor raises the mass-weighted $|\nabla v|$ at year 5 by a factor of 1.24–1.43. Over years 1–8 on the Upper Arkansas, the centroid of the top 5% of v lies 7–10 km east of the focus in the full model and 9–13 km with isotropic diffusion, but 3 km with the land cover flattened and under 1 km with neither. Carbondale repeats the elevation ordering of the low/high ratio more weakly. Around Estes Park every arm leaves the plains at the eastern edge almost untreated, so its inverted ratio of 0.42–0.49 reflects where the focus sits rather than either mechanism.

Table S4: The 2×2 ablation on each mesh at $\delta = 0.25$, landscape-average $R_0 = 3.5$, $c_4 = 0.5$. **D** is slope-anisotropic or isotropic ($\eta \equiv 1$), and the land cover is measured or flattened to its mean. Reductions are percentages against each arm's own baseline. "Mean v" is the mass- and block-weighted realized effort, and "efficiency" is deficit reduction in percentage points per unit of it. "Never" is the share of the mesh at $v = 0$ in all twenty blocks, and "low/high" is the ratio of time-mean effort in the lowest elevation quartile to that in the highest.

Mesh	**D**	Land cover	T_{intro} (yr)	Deficit	$\hat{J}$	Mean v	Effic.	Never (%)	Low/high
Upper Arkansas	aniso.	measured	10.15	−32.3	−19.9	0.41	79.6	55.4	3.20
	aniso.	flattened	9.55	−32.3	−20.0	0.50	64.6	49.9	1.20
	iso.	measured	11.15	−33.2	−20.2	0.48	69.7	46.7	2.29
	iso.	flattened	9.30	−33.1	−20.5	0.60	55.4	40.3	0.91
Carbondale	aniso.	measured	10.75	−33.1	−20.2	0.47	70.1	52.8	2.82
	aniso.	flattened	9.40	−32.2	−19.9	0.51	63.3	49.8	2.12
	iso.	measured	10.60	−34.0	−20.8	0.59	57.9	41.0	2.14
	iso.	flattened	9.30	−33.1	−20.5	0.64	51.8	37.3	1.56
Estes Park	aniso.	measured	9.80	−28.1	−16.9	0.36	77.3	63.1	0.49
	aniso.	flattened	9.65	−30.6	−18.6	0.41	75.1	57.9	0.42
	iso.	measured	9.55	−29.1	−17.5	0.47	61.7	50.9	0.49
	iso.	flattened	9.40	−31.8	−19.3	0.56	56.4	41.2	0.44

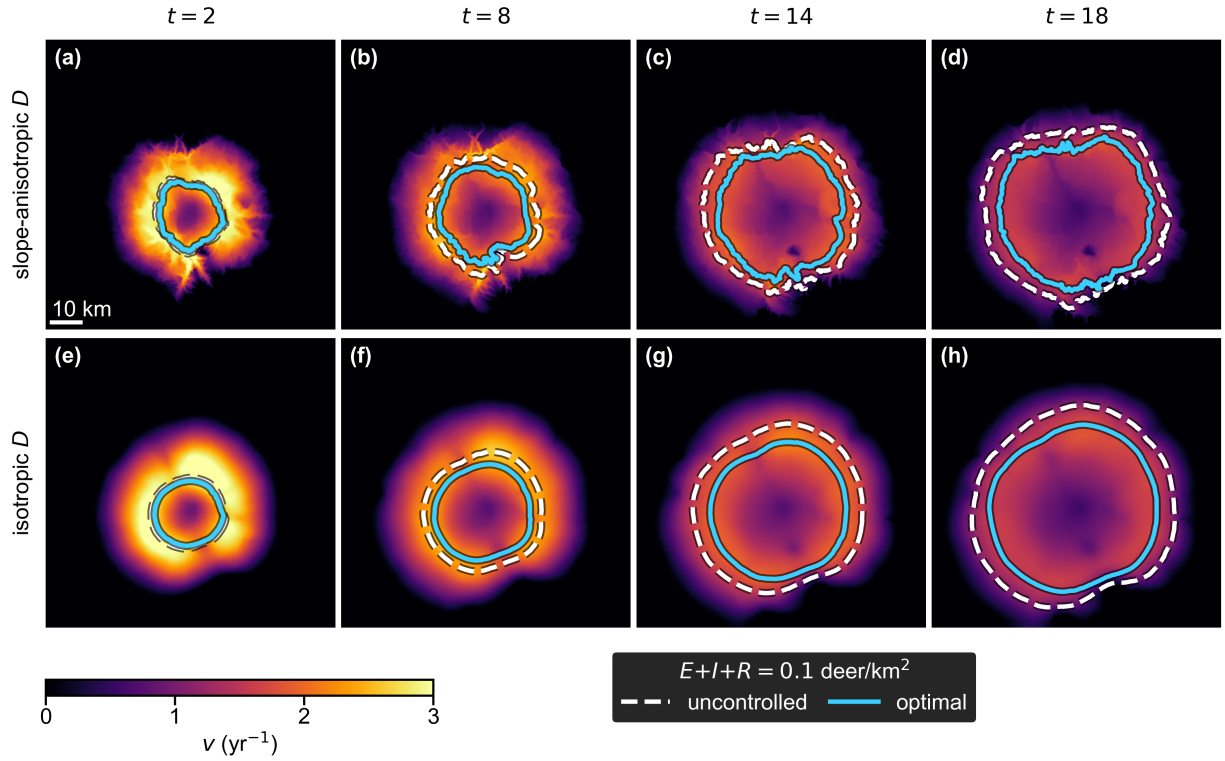


Figure S2: The ablation on the Carbondale mesh at $\widetilde{R_0} = 4.18$, on the same terms as Figure 6. The front spreads almost radially in both arms, and the heaviest effort stays within 2 km of the focus east to west.

S4 Verification and Further Results on the Disk

This section gives the verification behind Section 6.9, the handover state and uncontrolled outcome of every cell of the sweep, and the robustness checks summarized in Section 7.6.

Over 600 random states, including poor habitat and the $K < 0.01$ branch, the mesh-free check gives worst relative residuals of 7.0×10^{-10} on the adjoint transpose and 2.9×10^{-9} on the control gradient, at the truncation error of the central-difference reference, and recovers $S^* = K_0/\widetilde{R_0}$ to 2×10^{-16}. Table S5 gives the Taylor test, with directions scaled to unit root-mean-square so that ε is in the control's own units. The full-support direction certifies the discrete adjoint identity. The last-block direction isolates the continuation tail, whose cost reaches the gradient only through $\lambda(\cdot, T_c)$, so an error there is not diluted over all twenty blocks. The remainder reaches the round-off floor only at $\varepsilon = 10^{-6}$. Across the 12 optimizations of the sweep the projected-gradient residual (40) falls from 0.42–1.53 to 1.2×10^{-5}–1.7×10^{-4} (median 4.2×10^{-5}).

Table S5: Taylor test of the discrete gradient on the Upper Arkansas mesh (350,315 nodes, $T_c = 20$ yr, $T_{tail} = 10$ yr, $\Delta t = 0.05$ yr), at an interior control with $\hat{J}(v) = 1.0074 \times 10^6$. R_1 should fall at rate 2 down to the round-off floor $10^{-13}|\hat{J}| = 1.0 \times 10^{-7}$.

	full support		last block only	
ε	R_1	rate	R_1	rate
10^{-1}	5.2445×10^{2}	—	5.2517×10^{2}	—
10^{-2}	5.2445×10^{0}	2.00	5.2517×10^{0}	2.00
10^{-3}	5.2445×10^{-2}	2.00	5.2517×10^{-2}	2.00
10^{-4}	5.2445×10^{-4}	2.00	5.2517×10^{-4}	2.00
10^{-5}	5.2404×10^{-6}	2.00	5.2563×10^{-6}	2.00
10^{-6}	4.5601×10^{-8}	2.06	5.1091×10^{-8}	2.01
$\langle \nabla \hat{J}, d \rangle$	4.6207×10^{1}		-8.7811×10^{1}	

Table S6 gives the handover state and the uncontrolled outcome of every cell. The detection rule equalizes accumulated clinical burden but not the epidemiological state. Along δ it holds handover prevalence within a factor of 2.4–2.8 over an eightfold range of persistence, whereas a fixed twenty-year introduction would hand the control problem 6–17 times the prevalence at $\delta = 1$ as at $\delta = 0.125$. Across R_0 it cannot, and the infected load at handover spans a factor of 8.0 from corner to corner, from 37 to 296 animals. Slow cells hand over an environment-heavy state and fast cells a host-heavy one. Along the $R_0 = 5$ row, W falls from 138.7 to 78.1 while the number of infected animals more than doubles. Where the herd collapses fastest, the infection falls below 0.1 deer/km^2 everywhere once the first wave has crossed the disk, and at two cells a second wave spreads from the focus during the tail as the herd recovers.

Table S7 complements Table 4 with the change in $\hat{J}$, the change in cumulative incidence and the efficiency of the control. At $R_0 \leq 3.5$ a slower reservoir is cheaper to manage per point of benefit, with efficiency falling from 151.7 to 30.9 along δ at $R_0 = 2$. At $R_0 = 5$ it levels off at about 9 for $\delta \geq 0.5$. Cumulative incidence rises under control at 5 of 12 cells, by 7.8 to 16.6%, because the control keeps deer alive. At ($\delta = 1,\ R_0 = 5$), susceptible exposure $\iint S$ rises from 159 to 181 thousand deer-years, so more infections are counted against a larger herd.

The control rarely saturates. The space–time share at v_{max} is at most 4.3%, at ($\delta = 1,\ R_0 = 2$), and at or below 1.6% at nine of twelve cells. The c_4 threshold sits at 15% of the largest $\lambda_R R$ measured on the grid, 3.38.

For the transmission ratios, we reran the ($\delta = 0.25,\ R_0 = 3.5$) cell at $\varrho = 5$, where clinical

Table S6: The uncontrolled baseline per cell on the flat disk. Left: the handover state y^0, namely detection time (54), domain prevalence, infected animals and reservoir. Right: the outcome over $[0, T]$, namely the deficit integral priced by $\hat{J}$, cumulative incidence, infected animals at T, the mean force of infection (56), and the largest herd decline against S_∞, read from 2-yearly output.

		Handover state y^0				Uncontrolled outcome				
R_0	δ	T_{intro} (yr)	Prev. (%)	$E{+}I{+}R$ (deer)	W (p.u.)	Deficit (10^3 deer·yr)	Cum. inc. (deer)	$E{+}I{+}R$ at T	Hazard (56)	Decline (%)
2	0.125	19.05	0.24	36.8	88.4	15.0	3367	441	7.7	5.8
	0.25	15.55	0.36	54.3	71.5	40.5	8745	1175	21.2	17.9
	0.5	13.00	0.51	76.4	55.4	87.0	16637	1794	45.5	38.9
	1.0	11.25	0.67	100.5	40.0	131.9	20735	1254	64.7	48.2
3.5	0.125	10.55	0.56	83.6	123.1	96.4	17226	1980	48.4	47.4
	0.25	9.00	0.79	118.0	103.6	176.8	22278	973	80.8	76.2
	0.5	7.80	1.08	162.0	84.7	229.2	21396	493	95.9	79.6
	1.0	6.90	1.42	212.1	64.9	246.2	20526	747	99.6	81.3
5	0.125	7.90	0.84	126.4	138.7	192.3	22188	768	85.3	85.6
	0.25	6.95	1.15	172.7	119.4	255.6	20349	238	103.4	91.1
	0.5	6.15	1.54	230.9	100.0	286.0	18349	154	110.3	93.0
	1.0	5.50	1.98	295.7	78.1	293.0	17161	239	107.7	93.6

Table S7: Further measures of the optimal control on the flat disk, as percentage change against each cell's own baseline. "Efficiency" is deficit reduction in percentage points per unit of mean effort (Table 4).

R_0	δ	$\hat{J}$	Cum. inc.	Effic.
2	0.125	−16.2	−26.4	151.7
	0.25	−29.0	−38.2	82.4
	0.5	−34.9	−39.3	46.3
	1.0	−31.8	−27.5	30.9
3.5	0.125	−23.3	−24.0	38.2
	0.25	−18.6	−5.8	21.1
	0.5	−10.2	+7.8	13.3
	1.0	−5.1	+11.4	9.8
5	0.125	−15.5	−2.0	18.8
	0.25	−8.5	+8.5	11.9
	0.5	−4.9	+12.0	8.8
	1.0	−4.4	+16.6	9.0

animals shed twice as much while alive, and at $m = 2.6$ and 18.2 (Section 2.9). We test ϱ only upward, since $\varrho = 4$ already assumes that the stages shed alike while alive, and background mortality would lower it only to about 3.5. Raising ϱ to 5 raises the clinical share R_0^{clin}/R_0 from 60 to 65% and the recovered deficit from 31 to 34%, with almost no change in the dynamics. Changing m also changes the reproduction cycle, since the environmental route holds infection in W for $1/\delta$. At $m = 2.6$ the invasion growth rate r_{inv} rises from 0.38 to 0.46 yr^{-1} and the recovered deficit falls to 20%, far more than its clinical share of 56% explains. At $m = 18.2$ the cull sees about as much as at $\varrho = 5$ but recovers 37%, since the cycle is slower. The benefit is thus set first by the clinical share and then by the length of the reproduction cycle, as along δ in Table 4.

We measured the effects of tail truncation and time step on the Park Range test mesh of Section 6.7, at ($\delta = 0.25$, $\widetilde{R_0} = 2.37$) and $v_{\max} = 2$. Doubling the tail to $T_{\mathrm{tail}} = 20$ yr took the baseline and controlled deficits from 14071 and 8346 to 26847 and 16267, moving the reported reduction from 40.69 to 39.40%. Truncation inflates both arms and nearly cancels in the ratio. The uncontrolled objective varied by 0.17% across $\Delta t = 1/40$, 1/30 and 1/20 yr, non-monotonically as the discrete detection rule predicts, and three full optimizations agreed to 0.19% in $\hat{J}$ and 0.09% in realized effort.

References

Emily S. Almberg, Paul C. Cross, Christopher J. Johnson, Dennis M. Heisey, and Bryan J. Richards. Modeling routes of chronic wasting disease transmission: environmental prion persistence promotes deer population decline and extinction. *PLoS ONE*, 6(5):e19896, 2011. https://doi.org/10.1371/journal.pone.0019896.

Melia T. DeVivo, David R. Edmunds, Matthew J. Kauffman, Brant A. Schumaker, Justin Binfet, Terry J. Kreeger, Bryan J. Richards, Hermann M. Schätzl, and Todd E. Cornish. Endemic chronic wasting disease causes mule deer population decline in Wyoming. *PLoS ONE*, 12(10): e0186512, 2017. https://doi.org/10.1371/journal.pone.0186512.

Martha J. Garlick, James A. Powell, Mevin B. Hooten, and Leslie R. MacFarlane. Homogenization, sex, and differential motility predict spread of chronic wasting disease in mule deer in southern Utah. *Journal of Mathematical Biology*, 69(2):369–399, 2014. https://doi.org/10.1007/s00285-013-0709-z.

Chris Geremia, Michael W. Miller, Jennifer A. Hoeting, Michael F. Antolin, and N. Thompson Hobbs. Bayesian modeling of prion disease dynamics in mule deer using population monitoring and capture-recapture data. *PLoS ONE*, 10(10):e0140687, 2015. https://doi.org/10.1371/journal.pone.0140687.

Marie L. J. Gilbertson, Alison C. Ketz, Matthew A. Hunsaker, Daniel P. Walsh, Daniel J. Storm, and Wendy C. Turner. White-tailed deer habitat use and implications for chronic wasting disease transmission. *Wildlife Monographs*, 217(1):e70001, 2025. https://doi.org/10.1002/wmon.70001.

Juan Francisco Mandujano Reyes, Ting Fung Ma, Ian P. McGahan, Daniel J. Storm, Daniel P. Walsh, and Jun Zhu. Spatiotemporal causal inference with mechanistic ecological models: evaluating targeted culling on chronic wasting disease dynamics in cervids. *Environmetrics*, 36(2): e2901, 2025. https://doi.org/10.1002/env.2901.

Michael W. Miller, N. Thompson Hobbs, and Simon J. Tavener. Dynamics of prion disease transmission in mule deer. *Ecological Applications*, 16(6):2208–2214, 2006. https://doi.org/10.1890/1051-0761(2006)016[2208:DOPDTI]2.0.CO;2.

Michael W. Miller, Heather M. Swanson, Lisa L. Wolfe, Fred G. Quartarone, Sherri L. Huwer, Charles H. Southwick, and Paul M. Lukacs. Lions and prions and deer demise. *PLoS ONE*, 3 (12):e4019, 2008. https://doi.org/10.1371/journal.pone.0004019.

Alex Potapov, Evelyn Merrill, Margo Pybus, and Mark A. Lewis. Chronic wasting disease: transmission mechanisms and the possibility of harvest management. *PLoS ONE*, 11(3):e0151039, 2016. https://doi.org/10.1371/journal.pone.0151039.

Andrew Sharp and John Pastor. Stable limit cycles and the paradox of enrichment in a model of chronic wasting disease. *Ecological Applications*, 21(4):1024–1030, 2011. https://doi.org/10.1890/10-1449.1.

Arun Suresh, Zoe Shanley, Shane Hesting, Levi Jaster, Akila Raghavan, and Ram K. Raghavan. The direction and rate of spread of chronic wasting disease. *Frontiers in Veterinary Science*, 13: 1827624, 2026. https://doi.org/10.3389/fvets.2026.1827624.

James T. Tanner. The stability and the intrinsic growth rates of prey and predator populations. *Ecology*, 56(4):855–867, 1975. https://doi.org/10.2307/1936296.

U.S. Geological Survey. 1/3rd arc-second digital elevation models (DEMs) – USGS national map 3DEP downloadable data collection. U.S. Geological Survey, 2024a. URL https://www.sciencebase.gov/catalog/item/4f70aa9fe4b058caae3f8de5.

U.S. Geological Survey. Annual NLCD collection 1 science products (ver. 1.2, june 2026). U.S. Geological Survey data release, 2024b.